International Research Journal of Engineering Science, Technology and Innovation Vol. 1(1) pp. 1-13, April, 2012
Available online http://www.interesjournals.org/IRJESTI

Full Length Research Paper

Flow physics of a combined darrieus-savonius rotor using computational fluid dynamics (CFD)

R. Gupta[1], K.K. Sharma[2]

[1]Director, NIT Srinagar, Srinagar (INDIA).
[2]Associate Prof. (Research Scholar), deptt. of Mechanical Engg., NIT Silchar, Assam (INDIA).

Accepted 16 March, 2012

Vertical Axis Wind Turbine (VAWT) is self-starting, omni-directional, inexpensive, and especially viable in low wind speed regimes. Savonius, Darrieus, H-Darrieus, combined Savonius-Darrieus, and Darrieus-Savonius rotors are the types of VAWTs. The Darrieus rotor has low starting torque but provides high power coefficient for which it can be coupled to Savonius rotor that provides high starting torque. The combination of Darrieus and Savonius rotors thus exhibits high starting torque and high power coefficient. In this paper, an attempt was made to study the flow physics of a combined three-bladed, Darrieus-three-bucket-Savonius rotor using Fluent 6.0 CFD software. The height of the combined rotor was 20 cm. Four overlap conditions in the range of 10.87% to 25.87% were considered for the Savonius part of the combined rotor. Contours of relative speed magnitude and static pressure on various horizontal and vertical iso-planes were analysed as obtained from the CFD simulations. High performance of the combined rotor was attributed to the Darrieus rotor for the observed highest relative speed of the combined rotor near its top and also for the highest pressure and speed drop across the combined rotor at low overlap like 15.37%. Moreover, good aerodynamic performance of the combined rotor could be expected by the presence of the Darrieus rotor on top which having no wake been formed downstream of the combined rotor.

Keywords: Combined Darrieus-Savonius rotor, overlap, tip-speed ratio, CFD, flow physics

INTRODUCTION

Wind is an environment friendly renewable energy source whose continual tapping for power generation will improve the present scenario of climate change from green house gas emissions. It was estimated that roughly 10 million MW of energy are continuously available in the earth's wind. From the data released by Global Wind Energy Council (GWEC), it can be seen that as of now, wind energy generating countries have raised the net wind energy installed capacity to a record high of 194,390 MW (Global wind energy market, 2010). Wind energy is converted into mechanical power by wind turbines and then converted into electricity with the help of generator. Wind turbines are broadly classified into two types: Horizontal Axis Wind Turbine (HAWT) or propeller turbine and Vertical Axis Wind Turbine (VAWT). HAWTs are installed in high wind speed regime like the coastal areas. However, in places where wind speed is relatively low and varies appreciably with seasons, there is a major scope of VAWTs which are viable for low wind speed applications like small-scale electrification, pumping, aerating, heating, grinding etc. VAWT rotors are of different types, like Savonius, helical Savonius, Eggbeater Darrieus, H-Darrieus, combined Savonius-Darrieus or Darrieus-Savonius rotors etc. S.J. Savonius developed Savonius rotor in late twenties (Savonius, 1931). The concept is based on the principle of Flettner's rotor, which is formed by cutting a cylinder into two halves along the central plane and then moving the two semi-cylindrical surfaces sideways along the

Nomenclature

C_p, power coefficient; K, turbulent kinetic energy; ∇P, pressure gradient; $\vec{S}_m$, mass source; $\vec{V}_r$, relative velocity; $\bar{\bar{\tau}}$, stress tensor; μ, eddy viscosity; μ_t, turbulent viscosity; ε, turbulence dissipation rate; λ, tip speed ratio (TSR)

*Corresponding Author email: r_guptanitsil@yahoo.com

cutting plane so that the cross-section resembled the letter `S`. Savonius tested more than 30 different models of his rotor in the wind tunnel and also in open air to determine the best geometry. The best of the rotor models had a maximum power coefficient of 31% while that of the prototype was 37%. Between Sixties and the last decade, many researchers (Macpherson, 1972; Newman, 1974; Khan, 1975; Modi et al., 1984; Sivasegaram, 1978; Khan, 1988; Grinspan et al., 2001; Modi and Fernando, 1989; Alexander and Holownia 1978; Saylers, 1985; Sharma et al., 2005; Biswas et al., 2007). Had worked on different designs of Savonius rotor and evaluated their power coefficients from 'Between Sixties…. up to the 20%- 52%. Very few studies on the combined Savonius-Darrieus rotor have been reported in the available literature (Gavalda et al., 1990). Studied the performance of a combined two-bladed Savonius-Darrieus rotor and reported a maximum power coefficient of 0.35 for an overlap of 16.67%. The high starting torque of the combined rotor was caused by the reduction of the zones of negative starting torque (Wakui et al., 2005), obtained a maximum power coefficient of 0.18 for a combined configuration of three-bladed Darrieus and two-bucket Savonius rotor with the latter mounted below the former (Gupta et al., 2006). Evaluated the performance of a combined two-bucket Savonius and three-bladed Darrieus rotor within overlap range of 16.2%-25%. The maximum power coefficient was obtained as 0.25 at 20% overlap (Gupta et al., 2008), again made a comparative study between a three-bucket Savonius rotor and a combined three-bladed Savonius-Darrieus rotor within overlap range of 16.2%-35%. The maximum power coefficient of the combined rotor was higher than the Savonius rotor, and it was reported to be 0.51. Applications of CFD for the aerodynamic analysis of VAWT are found in the available literature (Debnath et al., 2009). Computationally evaluated the performance of the rotor design of (Gupta et al., 2008), using Fluent 6.0 CFD software. The result showed good matching of computational and experimental efficiencies for all overlap conditions (Gupta and Sharma 2011). Studied the flow physics of a three-bucket Savonius rotor using Fluent 6.0 CFD software, the flow physics of the rotor with overlap variations (12.3%- 25.8%) was analyzed with respect to pressure and velocity contours. The effect of overlap variation in the aerodynamic performance of the rotor was studied at the optimum overlap (19.8%), the highest performance of the rotor was derived due to favourable pressure and velocity variations across the rotor (Gupta and Biswas 2011). Computationally analyzed, the flow physics and aerodynamic performance of the rotor design of Gupta et al (2008). It was concluded that power augmentation of the combined rotor was caused by high aerodynamic lift-to-drag coefficient resulted from blade-vortex interactions at small overlap in the Savonius rotor.

Thus, it is seen that combined configuration of Savonius and Darrieus rotors has got better aerodynamic performance for which its power coefficient is higher than conventional Savonius rotor. The three-bladed combined configuration of the rotors produces higher power coefficient than their two-bladed combined configuration. Such combined rotors can be suitable for low wind speed applications also as it provides high starting torque (Gupta et al., 2006/ 2008). However, very few works have been reported on these combined rotors in the available literature. Further, it has also been observed that the aerodynamic performance and optimum overlap of the combined rotor are strongly controlled by the flow physics of the individual rotors (Gupta and Biswas 2011). Keeping these in perspective, in the present paper, the flow physics of a combined three-bladed-Darrieus-three-bucket-Savonius rotor was analyzed computationally by using Fluent 6.0 CFD software and the performance coefficients obtained from the numerical study are validated with the experimental results.

Physical model

The Darrieus rotor was a three-bladed system and that Savonius rotor was a three-bucket system. In the combined configuration of Darrieus-Savonius rotor, the buckets of the Savonius rotor were 8 cm in chord, 3 mm in thickness and 10 cm in height. The Darrieus rotor in the combined configuration was made up of aluminum strips of chord 12 mm, thickness 3 mm, height 10 cm. Therefore, height of the combined rotors was 20 cm. Rotor was fixed to the shaft using screw and bolt arrangement. Ball bearing was used to support the central shaft at the base of the rotor. Washers and nuts having knurled surfaces were used to create overlap between the buckets of the Savonius rotor. Overlap is the distance of the inner edge of the bucket from the axis of rotation assuming the arc is carried to the full semi-circle. Different overlap conditions like 10.87%, 15.37%, 21.37%, 25.87% etc were obtained by changing the overall diameter of the rotor. It has been seen in the past research works (Newman, 1974; Khan, 1975; Modi et al., 1984; Gavalda et al., 1990; Wakui et al., 2005; Gupta et al., 2006). That maximum performance from the Savonius rotor can be derived for overlap variation within 16% to 25%. The central shaft of the rotors was 1.5 cm in diameter and 25 cm in length. The base was 7 cm wide and 2.4 cm thick. Schematic diagram of the combined three-bladed-Darrieus-three-bucket-Savonius rotor is shown in figure 1.

Computational modeling

The three dimensional computational domain of the combined three-bladed-Darrieus-three-bucket-Savonius rotor along with the boundary conditions is shown in the figure 2 (a). The computational domain resembles the

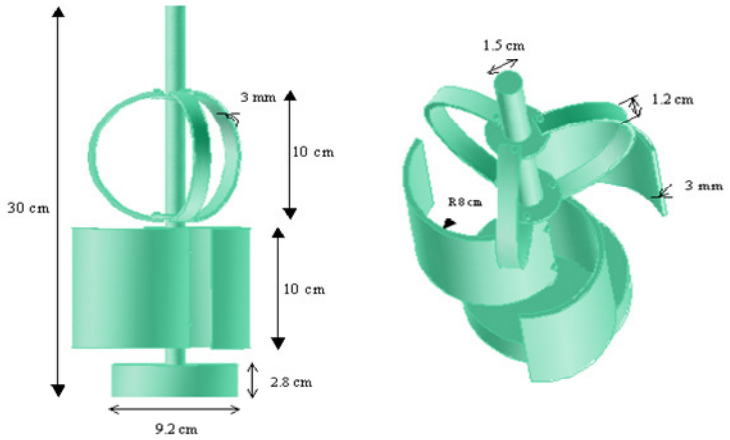

Figure1. Physical model of combined three-bladed-Darrieus-three-bucket Savonius rotor

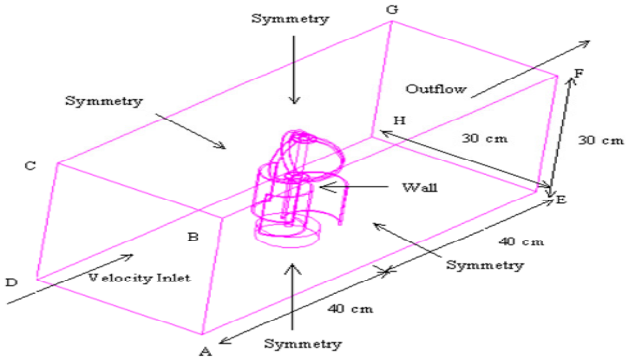

Figure 2 (a): Computational domain and boundary conditions of combined Darrieus-Savonius rotor

Table 1. Details of refinement levels of the combined Darrieus-Savonius rotor

Refining Level	No. of Nodes	No. of faces (Triangular)
1	52808	190017
2	58171	212366
3	60122	237897
4	63805	319592
5	65319	347526

original test section of the wind tunnel, which was 30cm x 30cm in cross-section. The length of the computational domain is 80 cm such that inlet and outlet faces are five times the bucket/blade diameter distance away from the central axis of the combined rotor. Wind **s**peed was considered on the inlet face ABCD, outflow was considered on the outlet face EFGH, symmetry condition was considered for the side walls (faces ABFE and CDHG) and bottom and top faces (ADHE and CBFG). And wall condition was considered for the blades, buckets and central shaft of the combined rotor. Computationally modeling was done in gambit of the Fluent 6.0 package. On the surrounding four faces of the computational domain, uniform grid spaces were taken. However, non-uniform meshing was done on the rotor. The density of mesh was kept high near the blade/bucket peripheries and their ends. This was done to capture the separated rotor vortices. Each mesh element is considered as a control volume. The unstructured tetrahedral mesh around the rotor within the computational domain is shown in the figure 2 (b). The grid independent limit computational mesh (Masson eta al., 1997). Was obtained by changing the resolution of mesh at all

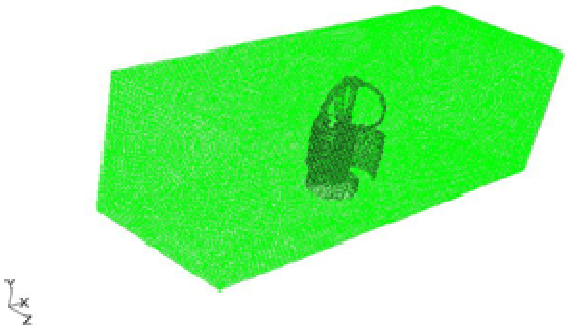

Figure 2 (b). Computational mesh of the combined Darrieus-Savonius rotor

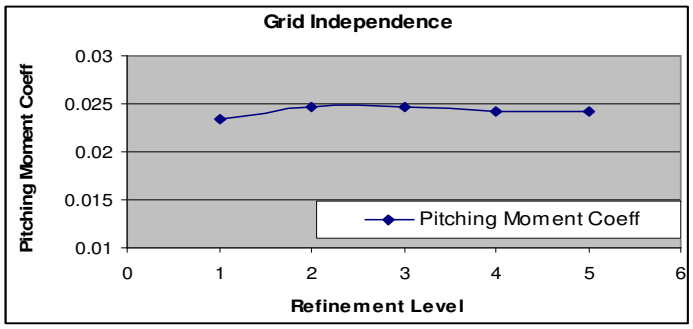

Figure 3. Variation of pitching moment coefficient with refinement levels of the grid of combined Darrieus-Savonius rotor

important areas of the rotor. Each refinement level was solved in Fluent with the same set of input parameters. The various levels of refinement used for the grid independence analysis of the combined rotor are shown in table 1. The variation of pitching moment coefficient of the combined rotor with respect to refinement levels is shown in the figure 3. The refinement level 4 of table 1 is considered for final simulation.

CFD Analysis of combined Darrieus-savonius rotor

The finite difference forms of continuity, Navier-Stokes and turbulence equations for incompressible flow of constant viscosity were solved by the in-built functions of the fluent CFD package. The equation for conservation of mass, or continuity, can be written in vector form as:

$$\nabla.(\rho \vec{V}\ ) = \vec{S}_m \qquad [1]$$

Where, value of $\vec{S}_m$ is zero for steady-state flow

The vectored momentum equation in terms of relative speed, $\vec{V}_r$ can be written as

$$\frac{\partial}{\partial t}(\rho \vec{V}_r) + \nabla.(\rho \vec{V}_r \vec{V}_r) + \rho(2\vec{\omega}\vec{V}_r + \vec{\omega}\vec{\omega}r) = -\nabla P + +\nabla.(\bar{\bar{\tau}}) \qquad [2]$$

According to the eddy viscosity concept of the Stokes' hypothesis for Newtonian fluids, the Reynolds stress tensor, $\bar{\bar{\tau}}$ can be expressed as

$$\bar{\bar{\tau}} = \mu[(\nabla \vec{V}_r + \nabla \vec{V}_r{}^T) - \frac{2}{3}\nabla.\vec{V}_r I] \qquad [3]$$

The two-equation turbulence model used for kinetic energy and dissipation rate transportation was realizable k-ε turbulence model. This model is fast and accurate in terms of predicting separated flow from the wind rotor**.** The modeled transport equations for *k* and ε are:

$$\frac{\partial}{\partial t}(\rho k) + \frac{\partial}{\partial x_i}(\rho k u_i) = \frac{\partial}{\partial x_j}\left[\left(\mu + \frac{\mu_t}{\sigma_k}\right)\frac{\partial k}{\partial x_j}\right] + G_k - \rho\varepsilon - Y_M \qquad [4]$$

$$\frac{\partial}{\partial t}(\rho \varepsilon) + \frac{\partial}{\partial x_i}(\rho \varepsilon u_i) = \frac{\partial}{\partial x_j}\left[\left(\mu + \frac{\mu_t}{\sigma_\varepsilon}\right)\frac{\partial \varepsilon}{\partial x_j}\right] + C_{1\varepsilon}\frac{\varepsilon}{k}(G_k) - C_{2\varepsilon}\rho\frac{\varepsilon^2}{k} \qquad [5]$$

Where $C_1 = \max\left[0.43, \frac{\eta}{\eta+5}\right]$, $\eta = S\frac{k}{\varepsilon}$ and rest are model constants [6]

In this study, steady state incompressible flow was considered. The numerical simulation was carried out by solving the conservation equations for mass,

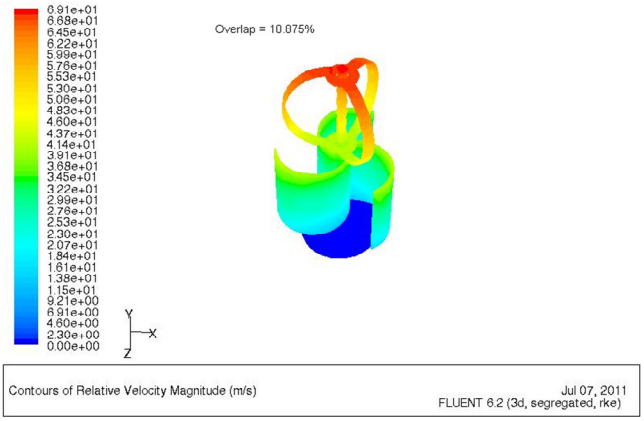

Figure 4 (a). Relative speed magnitude contour of the combined Darrieus-Savonius rotor for 10.87% overlap

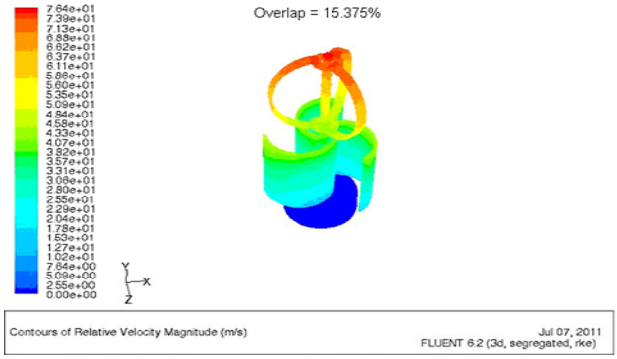

Figure 4 (b). Relative speed magnitude contour of the combined Darrieus-Savonius rotor for 15.37% overlap

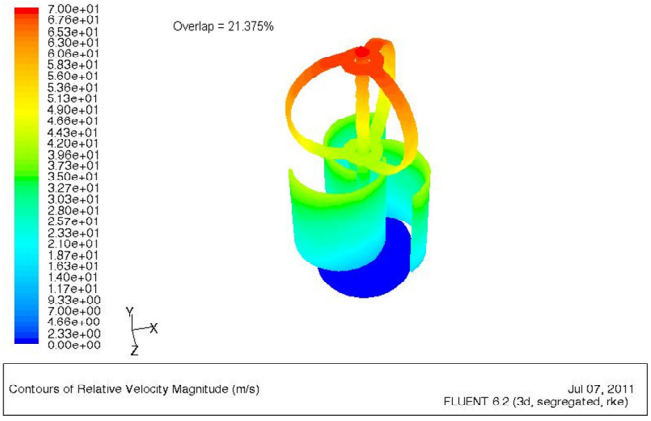

Figure 4 (c). Relative speed magnitude contour of the combined Darrieus-Savonius rotor for 21.37% overlap

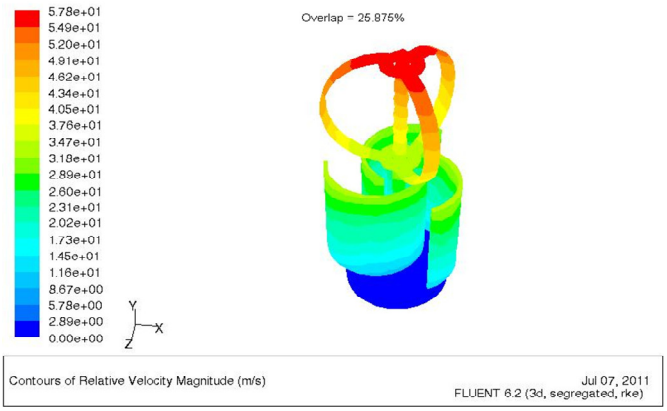

Figure 4 (d): Relative speed magnitude contour of the combined Darrieus-Savonius rotor for 25.87% overlap

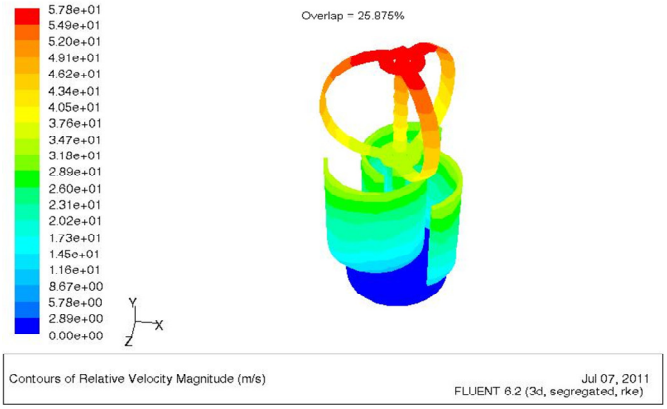

Figure 5 (a). Relative speed magnitude contour of the combined Darrieus-Savonius rotor for 10.87% overlap in ZX iso-planes

momentum and turbulence by using an unstructured-grid finite volume methodology coupled with moving mesh technique (FLUENT Inc. Fluent 6.0 documentation: user's guide, 2005). The method of dynamic grid or rotating reference frame was implemented in which the rotor is fixed in the view of an observer who is moving with the rotating frame of reference. Single rotating reference frame was considered, where the blades along with the support arms and the central shaft rotate relative to the incoming fluid stream. The sequential algorithm, Semi-Implicit Method for Pressure-Linked Equation (SIMPLE), was used for solving all the scalar variables. For the convective terms of the momentum equations and also for the turbulence equations**,** the second order upwind interpolating scheme (Versteeg and Malalasekera 1995). Was adopted.

Contour plot analysis of the combined darrieus-savonius rotor

The contour plot analysis gives an idea about the flow physics of a wind rotor, its aerodynamics and power production mechanism, solid-fluid interactions etc. In the present study, relative speed magnitude (speed of the rotor relative to wind) and static pressure contours of the combined rotor along with the pressure and speed contours on various iso-planes in horizontal and vertical positions were analysed. The contour plots were obtained for tip speed ratio at which the power coefficient of the combined rotor was the highest for each overlap condition. Figure 4(a) to figure4 (d) show the relative speed contours of the combined three-bladed-Darrieus-three-bucket-Savonius rotor for overlap conditions of 10.87%, 15.37%, 21.37% and 25.87%. Figure 5(a) to figure 5(d) show the relative speed contours in ZX iso-planes for the same overlap conditions, and figure 6(a) to figure 6 (d) show the corresponding relative speed contours in YZ iso-planes. Figure 7(a) to figure7 (d**)** show the static pressure contours of the rotor in ZX iso-planes for the aforesaid overlap conditions, and figure8 (a) to figure 8 (d) show the corresponding static pressure contours in YZ iso-planes.

Figures 4(a)-(d) show that speed of wind relative to the

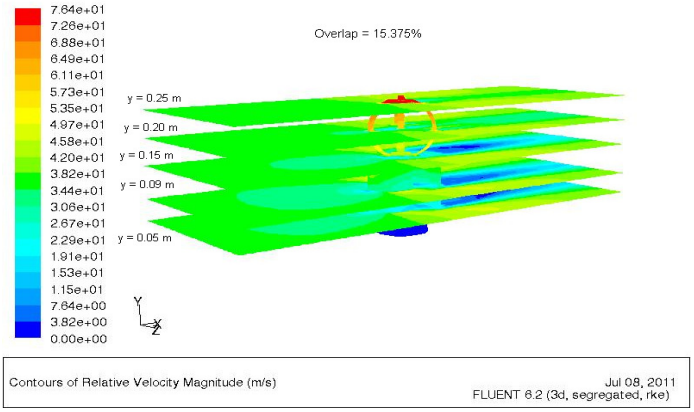

Figure 5 (b). Relative speed magnitude contour of the combined Darrieus-Savonius rotor for 15.37% overlap in ZX iso-planes

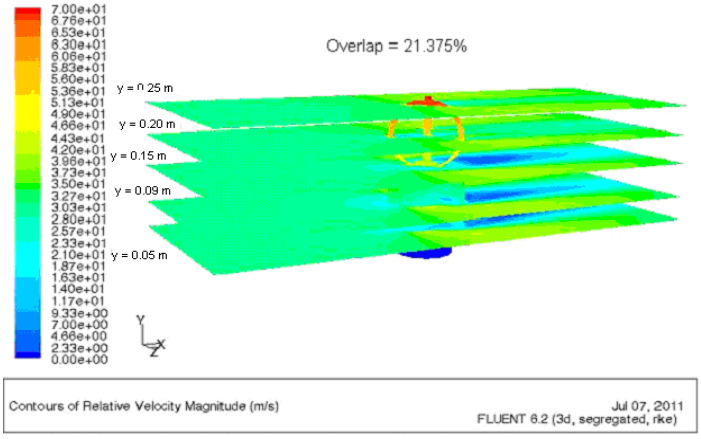

Figure 5 (c): Relative speed magnitude contour of the combined Darrieus-Savonius rotor for 21.37% overlap in ZX iso-planes

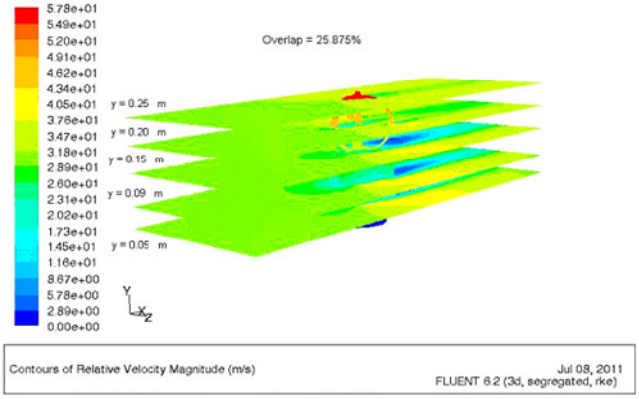

Figure 5 (d). Relative speed magnitude contour of the combined Darrieus-Savonius rotor for 25.87% overlap in ZX iso-planes

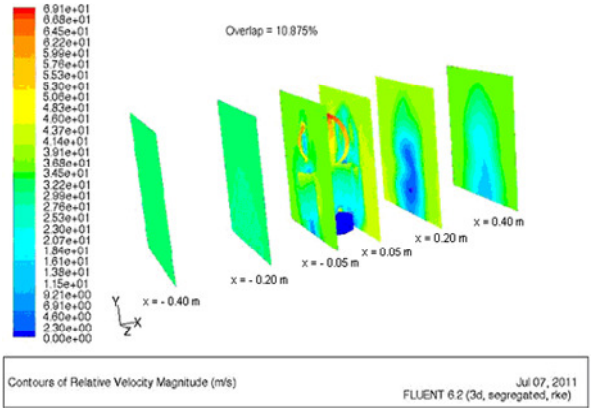

Figure 6 (a). Relative speed magnitude contour of the combined Darrieus-Savonius rotor for 10.87% overlap in YZ iso-planes

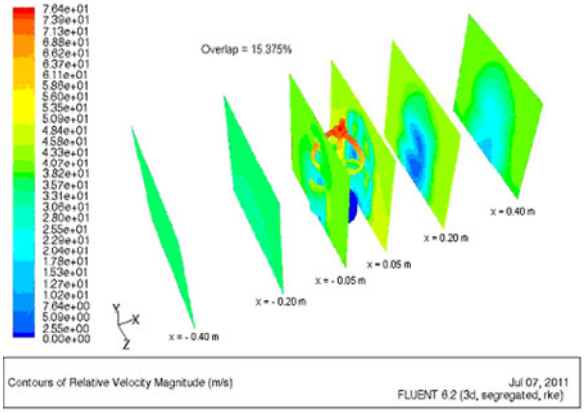

Figure 6 (b). Relative speed magnitude contour of the combined Darrieus-Savonius rotor for 15.37% overlap in YZ iso-planes

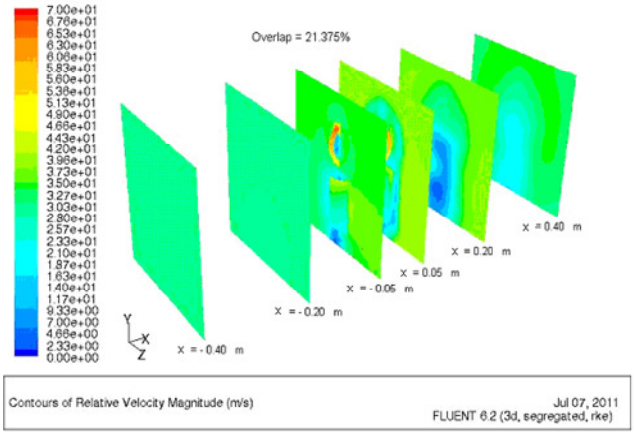

Figure 6 (c). Relative speed magnitude contour of the combined Darrieus-Savonius rotor for 21.37% overlap in YZ iso-planes

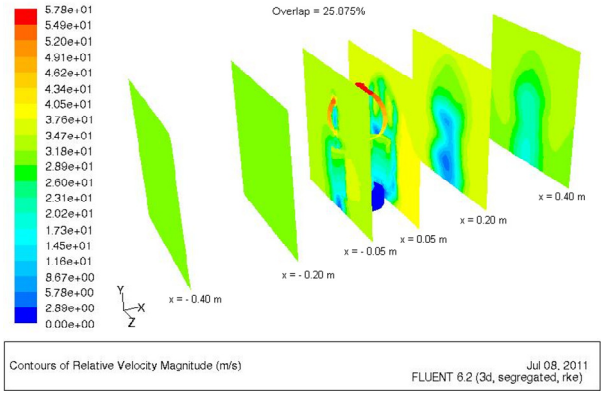

Figure 6 (d). Relative speed magnitude contour of the combined Darrieus-Savonius rotor for 25.87% overlap in YZ iso-planes

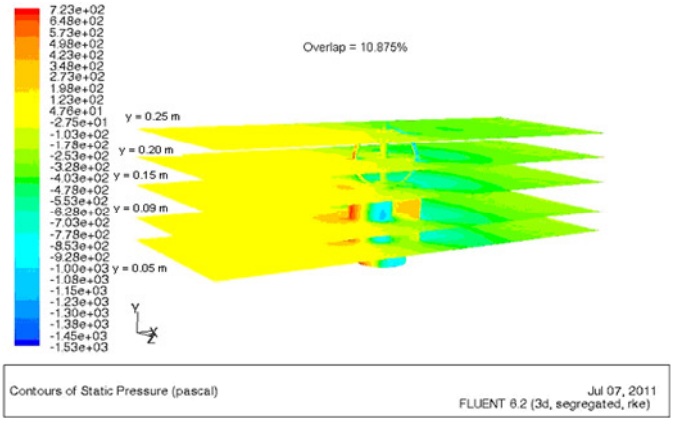

Figure 7 (a). Static pressure contour of the combined Darrieus-Savonius rotor for 10.87% overlap in ZX iso-planes

combined rotor increase in the upward direction from bottom to the top of the rotor, which is the maximum near the extreme height of the rotor. Thus, performance of the combined rotor will be controlled by the Darrieus rotor in the combined configuration as wind speed increases. These figures also show that, with the increase of overlap from 10.87% to 15.37%, the relative speed magnitude increases from the range of (2.3-69.1) m/sec to the range (2.55 - 76.4) m/sec. However, with further increase of overlap to 21.37% and then 25.87%, the range of variation of relative speed magnitude drops to (2.33 - 70) m/sec and (2.89 – 57.8) m/sec respectively.

The variations of relative wind speed in horizontal iso-planes (figure 5a-figure 5d**)** also show that speed increase in the upward direction plane wise. Further, in each iso-plane, relative speed magnitude decreases from upstream to downstream side of the rotor resulting in power extraction from wind by the rotor. The relative speed difference between the upstream and downstream sides of the combined rotor is the maximum at 15.37% overlap for which performance of the combined Darrieus-Savonius rotor will also be the maximum at that overlap condition. The relative speed magnitude contours in vertical iso-planes (figure 6a-figure 6d) also show the same trend in the variation of speed magnitude as the horizontal iso-planes. Further, presence of wake can be seen in the immediate downstream of the Savonius rotor, which diminishes gradually towards the end of the computational domain (at x = 0.40 m). This affects the performance of the Savonius rotor alone; however, no wake region is observed downstream the Darrieus rotor for which good aerodynamic performance of the combined rotor is possible by the presence of the Darrieus rotor on top.

The static pressure contours (fig.7a-fig.7d) in horizontal iso-planes (ZX-planes) clearly show that static pressure decreases from upstream side to the downstream side across the combined rotor, which results in useful lift for the rotor. At 10.87% overlap (figure 7a), static pressure decreases from 123 Pascal to -178 Pascal from upstream side to downstream side of the combined rotor**.** At 15.37% overlap (figure 7b), static pressure decreases from 240 Pascal to -114.

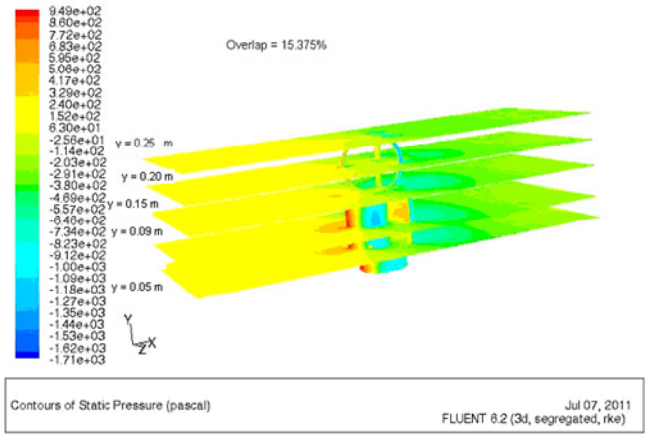

Figure 7 (b). Static pressure contour of the combined Darrieus-Savonius rotor for 15.37% overlap in ZX iso-planes

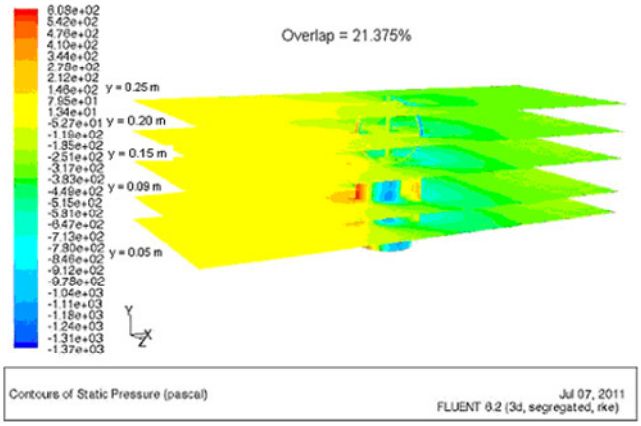

Figure 7 (c). Static pressure contour of the combined Darrieus-Savonius rotor for 21.37% overlap in ZX iso-planes

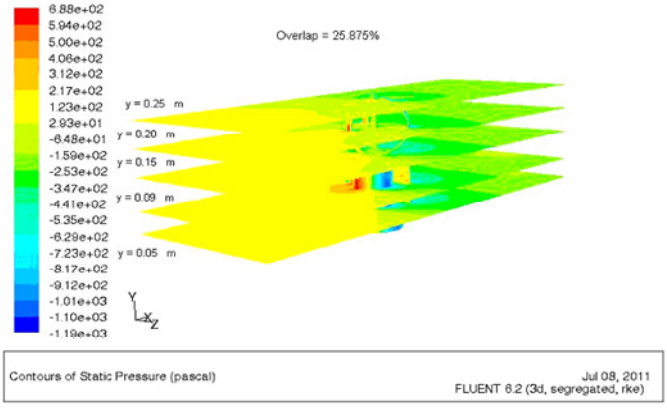

Figure 7 (d). Static pressure contour of the combined Darrieus-Savonius rotor for 25.87% overlap in ZX iso-planes

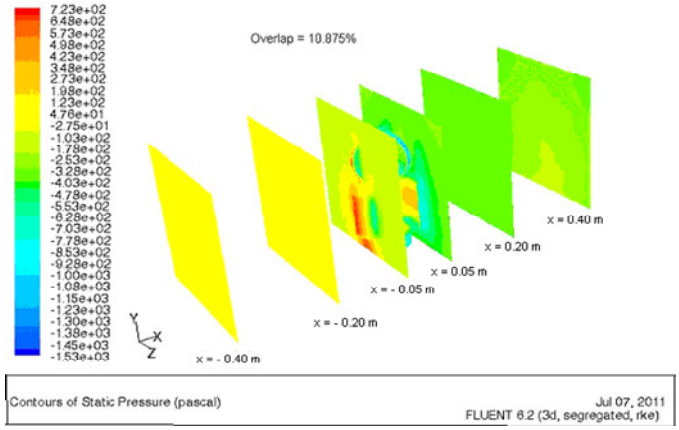

Figure 8 (a). Static pressure contour of the combined Darrieus-Savonius rotor for 10.87% overlap in YZ iso-planes

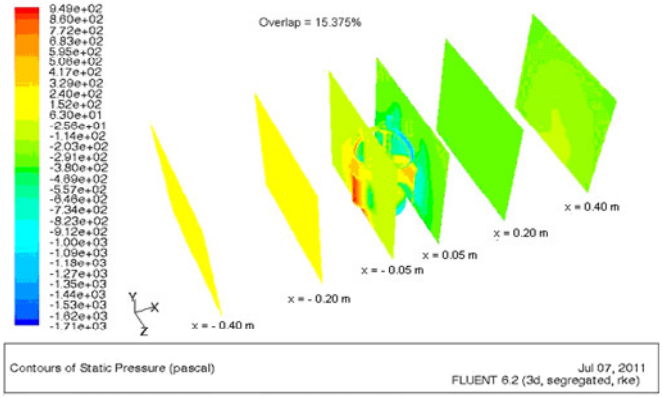

Figure 8 (b). Static pressure contour of the combined Darrieus-Savonius rotor for 15.37% overlap in YZ iso-planes

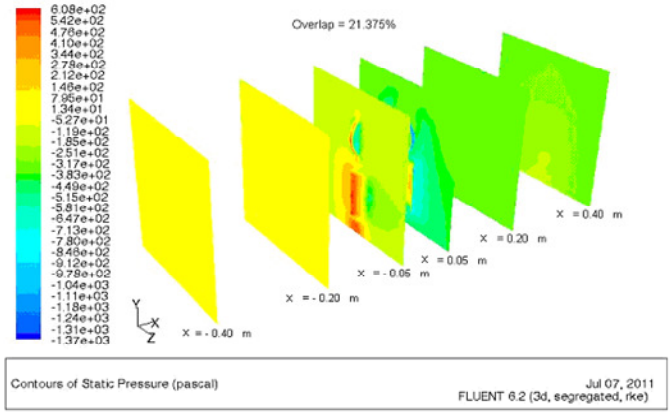

Figure 8 (c). Static pressure contour of the combined Darrieus-Savonius rotor for 21.37% overlap in YZ iso-planes

Pascal from upstream side to downstream side. Therefore, with increase in overlap from 10.87% to 15.37%, the drop of static pressure across the combined rotor increases. Now at 21.37% overlap, static pressure decreases from 79.5 Pascal to -185 Pascal from upstream side to downstream side; hence compared with 15.37% overlap, change of static pressure across the combined rotor decreases. And at 25.87% overlap, it further decreases; therefore, 15.37% is the optimum overlap at which static pressure difference across the rotor is the highest. The static pressure contours in vertical iso-planes (figure 8a-figure 8d) also show the same trend in the variation of static pressure as the horizontal iso-planes.

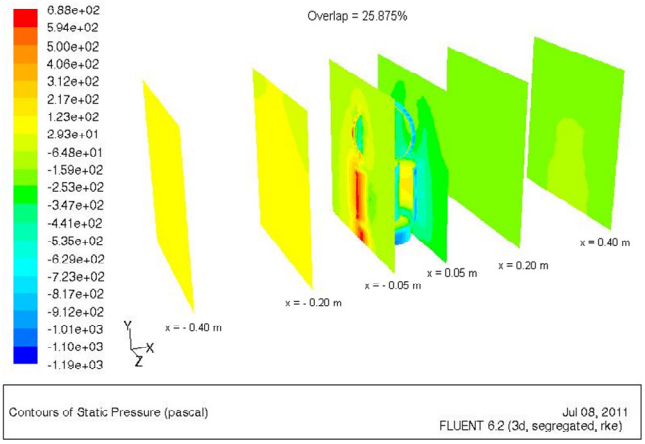

Figure 8 (d). Static pressure contour of the combined Darrieus-Savonius rotor for 25.87% overlap in YZ iso-planes

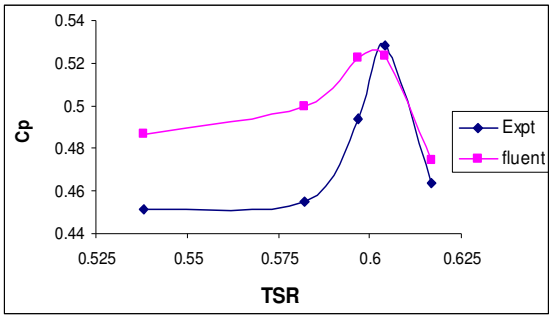

Figure 9 (a). Comparison of variation of computational C_p and experimental C_p with TSR for 15.37% overlap

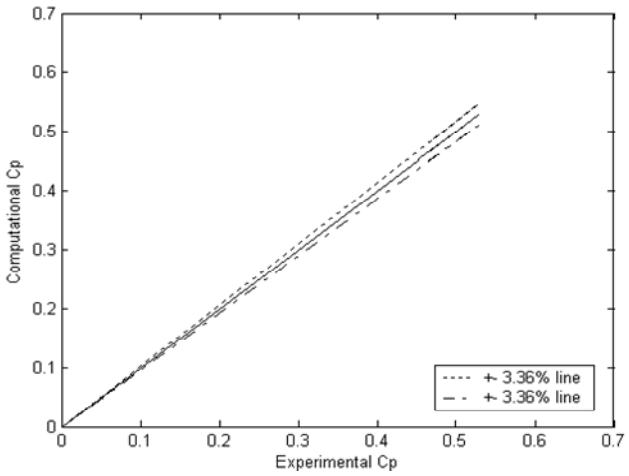

Figure 9 (b). Percentage deviation of computational C_p from the experimental C_p

Comparison of Power Coefficient (C_p) with Experimental Values

The reliability of numerical modelling for the performance study of the combined rotor can be proven if the computational results are validated with the experimental results. In the present case, the variation of power coefficient (C_p) with respect to tip speed ratio

(λ), TSR is compared with the corresponding experimental result at 15.37% overlap as shown in figure 9. The trend in the variation of C_p is exactly similar to the experimental trend. In both the cases, C_p increases with the increase of TSR up to a certain extent and then both decrease with further increase of the latter. The agreement between the two results is within ± 3.36%.

CONCLUSION

Flow physics analysis clearly shows the significance of mounting the Darrieus rotor on top of Savonius rotor by two ways: firstly, the Darrieus rotor stays clear of the wake of the Savonius rotor, which is seen in its immediate downstream and secondly, wind speed relative to the combined rotor increases from bottom to its top, which is maximum in the proximity of the blades of the Darrieus rotor. Therefore good aerodynamic performance of the combined rotor for wake free zone in the downstream of the Darrieus rotor at increased wind speed, and high power coefficient as controlled by the increased wind speed near the Darrieus blades are the benefits of this combined configuration.

Flow physics analysis also shows the effect of overlap variation on the performance of the rotor. At the optimum overlap of 15.37%, power coefficient from the numerical modelling was obtained within an agreement of ± 3.36% with respect to the experimental result.

REFERENCES

Alexander AJ, Holownia BP (1978). "Wind tunnel test on a Savonius rotor". Journal of Industrial Aerodynamics. 3: 343-351.

Biswas A, Gupta R, Sharma KK (2007). "Experimental Investigation of Overlap and Blockage Effects on Three-Bucket Savonius Rotors". J. Wind Eng. 31 (5): 363–368.

Debnath BK, Biswas A, Gupta R (2009). "Computational fluid dynamics analysis of a combined three-bucket Savonius and three-bladed Darrieus rotor at various overlap conditions". Int. J. Renewable and Sustainable Energy 1:033110,

FLUENT Inc. Fluent 6.0 documentation: user's guide; (2005).

Gavalda J, Massons J, Diaz F (1990). "Experimental study on a self adapting Darrieus-Savonius wind machines". J. Solar and Wind Technolo. 7(4): 457-461.

Global wind energy market as of (2010). Press release of Global Wind Energy Council (GWEC).

Grinspan AS, Kumar PS, Mahanta P, Saha UK, Rao DVR, Bhanu GV, (2001). "Design, development and testing of Savonius wind turbine rotor with twisted blades". Proceedings of 28th National Conference on Fluid Mechanics and Fluid Power, Chandigarh, Dec 13-15, pp. 428-431.

Gupta R, Biswas A (2011). "CFD Analysis of Flow Physics and Aerodynamic Performance of a Combined Three-bucket Savonius and Three-bladed Darrieus Turbine". Int. J. Green Ener. 8: 209–233.

Gupta R, Biswas A, Sharma KK (2008). "Comparative study of three-bucket Savonius turbine with combined three-bucket-Savonius-three-bladed-Darrieus turbine". J. Renewable Ener. 33: 1974–1981

Gupta R, Das R, Sharma KK (2006). "Experimental study of a Savonius-Darrieus wind machine". Proceedings of the International Conference on Renewable Energy for Developing Countries, University of Columbia, Washington DC.

Gupta R, Sharma KK (2011). "Flow Physics of a Three-Bucket Savonius Rotor using Computational Fluid Dynamics (CFD)". Int. J. Res. in Mech. Eng. Technol. (IJRMET). 1(1): 46-51.

Khan MH (1975)."Improvement of Savonius Rotor-windmill". M.S. thesis, University of the Phillipines, Lasbonas.

Khan MH, (1988). "Model and prototype performance characteristics of S-rotor wind mills". J. Wind Eng. 12: 59-75.

Macpherson RB (1972). "Design, Development and testing of Low Head High Power coefficient Kinetic Energy Machine".M.Sc Thesis, University of Massachusetts, Amherst, M.A.

Masson C, Ammara I, Paraschivoiu I (1997). "An aerodynamic method for the analysis of isolated horizontal-axis wind turbines". Int. J. Rotating Mach. 3: 21-32.

Modi VJ, Roth NJ, Fernando MSUK (1984). "Optimal configuration studies and prototype design of a wind energy operated irrigation system. J. Wind Eng. and Industrial Aerodynamics 16: 85-96.

Modi VJ, Fernando MSUK, (1989). "On the performance of the Savonius wind turbine". ASME J. Solar Eng. 11: 71-76.

Newman BG (1974)"Measurement on a Savonius rotor with variable gap". Proceeding of Sherbrook University Symposium on wind energy", Sherbrook Canada, pp 116

Savonius SJ (1931). "The S-rotor and its application" J. Mech. Eng. 53(5): 333-338

Saylers AT (1985). "Blade configuration optimization and performance characteristics of a simple Savonius rotor" Proceedings of Institute of Mechanical Engineers. 199: 185-191.

Sharma KK, Gupta R, Singh SK , Singh, SR (2005). "Experimental investigation of the characteristics of a Savonius wind turbine". J. Wind Eng. 29(1): 77-82.

Sivasegaram S (1978) "Secondary parameters affecting the performance of resistance type vertical axis wind rotors". Wind Engg, vol (2) pp 49-58.

Versteeg HK, Malalasekera W (1995). "An introduction to computational fluid Dynamics, the finite volume method". In: Longman Scientific and Technical, New York, 132

Wakui T, Yoshiaki T, Takumi H, Toshio N **(**2005). "Hybrid con figuration of Darrieus and Savonius turbines for stand-alone wind turbine-generator system". J. Elect. Eng. in Japan. 150(4): 13-22